Arsenic Removal by Zerovalent Iron

A Field Study of Rates, Mechanisms and Long-Term Performance

Dimitrios Vlassopoulos[1], Nelson Rivera[2], Peggy A. O'Day[2], Michael T. Rafferty[1] and Charles B. Andrews[1]

[1]S.S. Papadopulos & Associates, Inc., 815 SW 2nd Ave., Portland, OR 97204
[2]School of Natural Sciences, University of California, Merced, CA

Zerovalent iron (ZVI) is an effective medium for removal of arsenic (As) from water. A performance evaluation was conducted at a field site where shallow groundwater is contaminated by As at mg/L levels. Field column tests show that As removal follows pseudo first-order kinetics, with a half-life on the order of 5 minutes. Steady-state column effluent concentrations decreased with increasing retention time for retention times shorter than 45 minutes, but were independent of retention time for longer retention times, indicating a steady-state uptake reaction. Spectroscopic and microscopic characterizations of unreacted and reacted material show that metallic iron is partially oxidized to maghemite (γ-Fe_2O_3) in the unreacted material and that arsenic is incorporated into an Fe(III) oxyhydroxide structure during reaction with groundwater. These results suggest that As uptake is controlled by the rate of incorporation of arsenic into Fe(III) oxyhydroxide as it forms during oxidation of

maghemite. To evaluate long-term performance, a prototype in-ground reactor (1.8 m^3 iron bed) was built and operated over a one-year period (~4,400 pore volumes) to treat groundwater with ~3 mg/L As. Initially, effluent As concentrations were less than 10 μg/L, but gradually increased over time as As accumulated on the reactive media. Between ~1,600 and 2,200 pore volumes, preferential pathways began to develop within the reactor, resulting in significant flow channeling and incomplete As removal.

In recent years, ZVI has received considerable attention as a reactive medium for removal of a variety of contaminants from water (*1*, and references therein). Technologies based on ZVI for As removal are of particular interest, in view of the strong chemical affinity of Fe for As, and potential reduction in treatment costs relative to existing alternatives such as chemical precipitation/coagulation and ion exchange. Numerous studies (*2-7*) have demonstrated As removal by ZVI in batch and flow-through systems. These studies have shown that the arsenic removal mechanism is closely linked to the formation of iron corrosion products.

Aqueous corrosion of elemental iron is an oxidative dissolution process, and proceeds both aerobically (coupled to oxygen consumption):

$$Fe^o + ½O_2 + 2H^+ = Fe^{++} + H_2O \quad (1)$$

as well as anaerobically (coupled to hydrogen evolution):

$$Fe^o + 2H^+ = Fe^{++} + H_{2(g)} \quad (2)$$

These reactions produce an increase in pH and dissolved iron concentration and a decrease in redox potential. Depending on water chemistry, Fe(II) can be further oxidized to Fe(III). With increasing degree of oxidation, solid corrosion products can include $Fe(OH)_2$, mixed Fe(II/III) oxides or hydroxides (magnetite, green rusts), and FeOOH polymorphs. Arsenic exhibits a strong affinity for sorption on green rusts (*8,9*), which are intermediate products of iron oxidation. Under oxidizing conditions, green rust will transform to ferric oxyhydroxide phases (*8*), in which arsenic can ultimately be sequestered by adsorption or co-precipitation (*10,11*). Furthermore, solid-phase spectroscopic and solution-phase speciation evidence indicates that As(V) does not directly participate as an oxidant in iron corrosion and therefore reduction of As(V) to As(III) is not expected to be significant (*4,9*).

Here we present results of an *in situ* groundwater treatment study conducted at a former pesticide manufacturing site in New Jersey where shallow groundwater in a perched zone is affected by arsenic at concentrations of up to several mg/L. Column tests were performed in the field to develop design and operating parameters for a prototype in-ground reactor. The reactor was initially operated and monitored over a one-year period to evaluate long-term performance. Characterization of reaction products and evaluation of uptake rates in the field are discussed in terms of a proposed reaction mechanism.

Materials and Mehtods

The granular ZVI used in this study was obtained from Connelly-GPM (Chicago, IL). The ZVI is fairly uniform in grain size (-8 to +20 mesh, or 0.84 to 2.38 μm) and has a relatively high specific surface area (1.8 m^2/g). A typical analysis yields (% by weight): Fe 89.8, C 2.85, Mn 0.6, S 0.107, P 0.132, Si 1.85, Ni 0.21, Cr 0.17, Mo 0.15, Ti 0.004, Cu 0.2, Co 0.003, and O content up to 3.9 % (by difference).

ZVI was mixed 50% by weight (approximately 1:3 by volume) with coarse quartz sand. The porosity of the mixture was measured at ~50%.

Field Column Tests

Three flow-through vessels were used: a 57-L canister, a 75-L canister, and a 10-cm diameter by 60-cm long (~4 L) PVC column. A known volume of the ZVI/sand mixture was packed between layers of pea gravel and the vessels were sealed. Groundwater was pumped to an equalization tank, and from there it was pumped to the reactor vessel. Each of the tests consisted of pumping groundwater through the vessel in upflow mode at a constant flow rate, which was varied between tests (0.07 – 2 L/min). This allowed the hydraulic residence time within the ZVI layer to be varied between 1 minute and 5 hours. Each test was run for between one and several days, depending on the flow rate.

Influent and effluent water temperature, pH, and specific conductance were monitored continuously with multi-parameter sensor/datalogger systems equipped with flow-through cells. Redox potential and dissolved oxygen in both influent and effluent were also measured periodically. Automatic samplers were used to collect influent and effluent water samples at regular intervals. Water samples were analyzed for As by inductively coupled plasma-optical emission spectroscopy (ICP-OES) and graphite furnace-atomic absorption (GF-AAS) (detection limits of 50 and 2 μg/L, respectively) and Fe by ICP-OES (detection limit of 20 μg/L).

Solid Phase Characterization

Following completion of the field column tests, reactive media samples were recovered for solid phase and spectroscopic studies. Since surface reactions were of interest, the reacted ZVI was sonified for an hour to collect the fine fraction from the surface. The fine material was recovered using a 0.45 μm filter. Subsamples of the fines were digested in *aqua regia* and analyzed by GF-AAS for As and Fe.

For X-ray absorption spectroscopy (XAS) analysis, samples were mounted wet into a teflon sample holder, and sealed with mylar tape. Bulk Fe K-edge XAS data were collected at the Stanford Synchrotron Radiation Laboratory to determine Fe phases based on the local atomic coordination around Fe atoms. Samples were run on beamline 2-3 at room temperature and on wiggler beamline 4-1 at cryogenic temperatures (15-20 K). All XAS data were collected using a Si(220) monochromator crystal and a vertical beam size of 1 mm. Energy was calibrated using the first inflection on the absorption edge of iron metal foil, which was set at 7112 eV. X-ray Absorption Near Edge Structure (XANES) and Extended X-ray Absorption Fine Structure (EXAFS) to k = 13 $Å^{-1}$ were collected and analyzed using EXAFSPAK (*12*) with theoretical phase shift and amplitude functions calculated with FEFF (*13*). XANES spectra were least-squares fit with linear combinations of reference iron compounds from a previously analyzed library (*14*). Energy was treated as an adjustable parameter; fits with energy shifts of greater than 1 eV were rejected. EXAFS spectra were analyzed by background subtraction and non-linear least-squares fits on a shell-by-shell basis by methods described previously (*14-16*).

The particle size and morphology of the iron media before and after reaction were examined by scanning electron microscopy (SEM) and energy dispersive spectrometry (EDS) for spot elemental analysis. Samples were mounted on aluminum alloy stub mounts with double-stick carbon tape. The SEM used was an FEI XL-30sFEG housed at the University of California, Davis. The microscope was operated at 20 kV with a working distance of 6 mm, a beam diameter of 2.6 nm, and 617 pA for the EDS analysis.

In-Ground Reactor

Design and Construction. Rate constants for As removal derived from the field column tests were used to design the full-scale prototype, which was intended to treat up to 40 L/min of water containing dissolved As at an average concentration of 3 mg/L. Figure 1 is a schematic diagram of the reactor. Contaminated groundwater is collected in a perforated drain pipe and is piped to the reactor through an in-ground, gravity flow system that isolates the flow

stream from surrounding groundwater. Water flows through a totalizing flow meter into the reactor and is discharged from the reactor into a limestone gravel trench. The reactor, constructed from a 3.5 m^3 concrete vault, was installed between 2.1 and 3.4 meters below ground surface. Treatment occurs within a 1.8 m^3 bed containing approximately 3400 kg of the ZVI/sand mixture. Gravel chambers are located at each end of the concrete vault to distribute the flow across the iron bed. Sampling ports are installed in the influent and effluent piping, and multilevel monitoring points are also installed at four locations within the reactor.

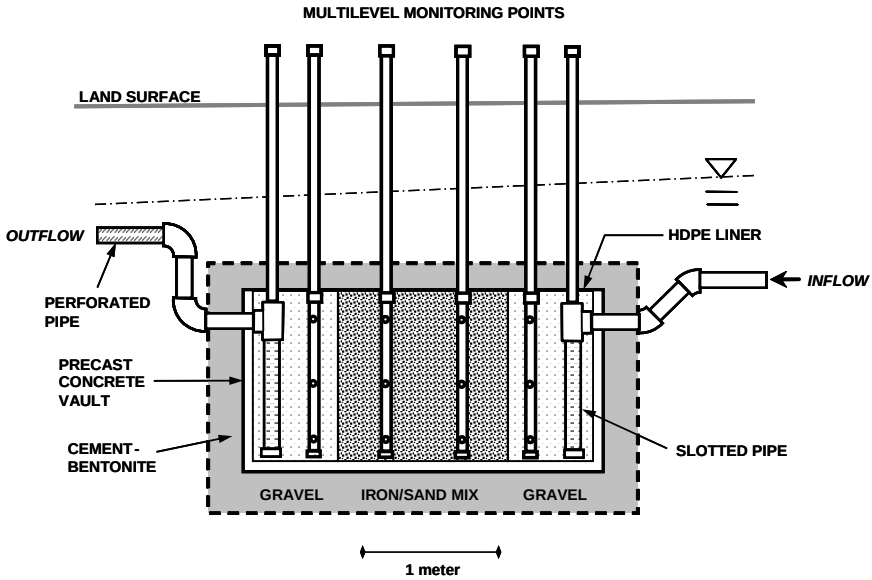

Figure 1. Schematic cross-section of in-ground reactor. The general location of the water table at time of construction is indicated by the sub-horizontal dot-dash line.

Monitoring. Samples from the influent, effluent, and interior monitoring points were collected periodically using a peristaltic pump fitted with disposable polyethylene tubing and operating at a low flow rate (<100 mL/min). Water temperature, specific conductance, pH, dissolved oxygen, redox potential (ORP) turbidity, and ferrous iron were measured in the field. Samples from influent, effluent and interior sampling ports were analyzed for total and dissolved As and Fe, major ions, Al, Mn, SiO_2 and H_2S. Water levels were also measured at each of the sampling ports to monitor hydraulic changes in the system.

Results

Field Column Tests

Influent As concentrations remained fairly constant over the duration of the tests, with a mean of 3.0 mg/L. Figure 2 shows steady-state effluent concentration as a function of retention time. Effluent As concentrations were generally less than 10 μg/L for tests with residence times longer than 47 minutes, but longer residence times did not appear to further decrease effluent As concentrations. For residence time tests shorter than ~45 minutes, higher effluent As concentrations were generally observed. The relationship between effluent arsenic and retention time is consistent with a combination of a first-order kinetic process (mass transfer) and an equilibrium partitioning as proposed in (*7*). Although there is some scatter in the short retention time data which may be attributed to differences between the reactors used and/or to aging of the ZVI over the duration of the tests, a first-order rate constant of 0.13 minute^{-1} is conservatively estimated, which corresponds to a half-life of arsenic in the column of approximately 5.3 minutes.

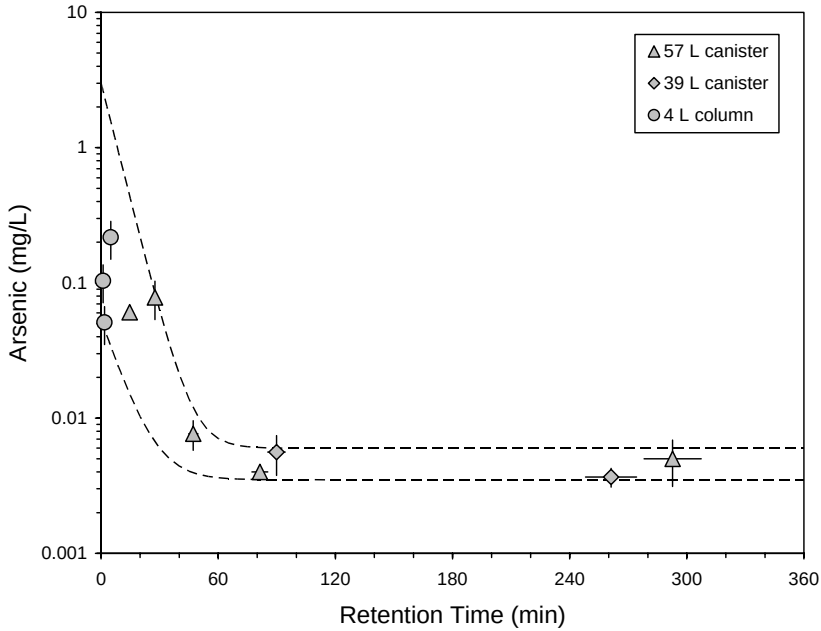

Figure 2. Steady-state column effluent arsenic concentration as a function of retention time. Dashed lines are upper and lower bound calculations assuming a combination of 1st-order removal rate and equilibrium partitioning.

Solid Phase and Spectroscopic Studies

Samples from the field column tests were analyzed by XANES and EXAFS spectroscopy at the Fe K-edge to examine iron phases before and after reaction with the groundwater. XANES analyses of unreacted ZVI and two samples of reacted material recovered from column tests showed differences in their spectral features, which are best seen in first-derivative spectra (Figure 3(a)). A distinct difference in the spectra occurs around 7130 eV where the unreacted ZVI exhibits a shoulder, wheareas the reacted ZVI has no such feature. This shoulder is also seen in the maghemite reference spectrum but not in iron oxyhydroxide reference spectra. There is no evidence in the unreacted iron spectrum for the presence of magnetite or iron metal, which were detected by XAS in a previous study (*5*), probably because fine surface material rather than bulk material was analyzed in this study. The unreacted iron spectrum was well fit with two components – maghemite (γ-Fe_2O_3), which contains both Fe(II) and Fe(III), as the dominate phase (81%), and a smaller component (19%) of an Fe(III) oxyhydroxide phase (Table 1). Because of the similarity in XANES spectral features among the Fe(III) oxyhydroxide compounds ferrihydrite (amorphous $Fe(OH)_3$), goethite (α-FeOOH), and lepidocrocite (γ-FeOOH), these phases cannot be distinguished by XANES analysis alone (*14*). Fits to the reacted iron spectra with maghemite were poor. Reacted iron spectra were well fit with a single Fe(III) oxyhydroxide component, as shown in Figure 3(b). Addition of a second component did not improve the fit significantly, and similar fits to the XANES spectra were obtained using ferrihydrite or goethite as the reference compound.

Table 1. XANES fit results for unreacted and reacted ZVI

Sample	*Reference compound*	*Fraction*	*Energy shift (eV)*	*[As][a] (mg/kg)*
Unreacted	Maghemite	81 %	0.65	
	Lepidocrocite	19 %	0.24	
Reacted #1	Lepidocrocite	100 %	0.05	450
Reacted #2	Lepidocrocite	100 %	0.09	250

[a]Concentrations of As by acid digestion, analysis by GF-AAS; detection limits for As were 6.25 mg/kg.

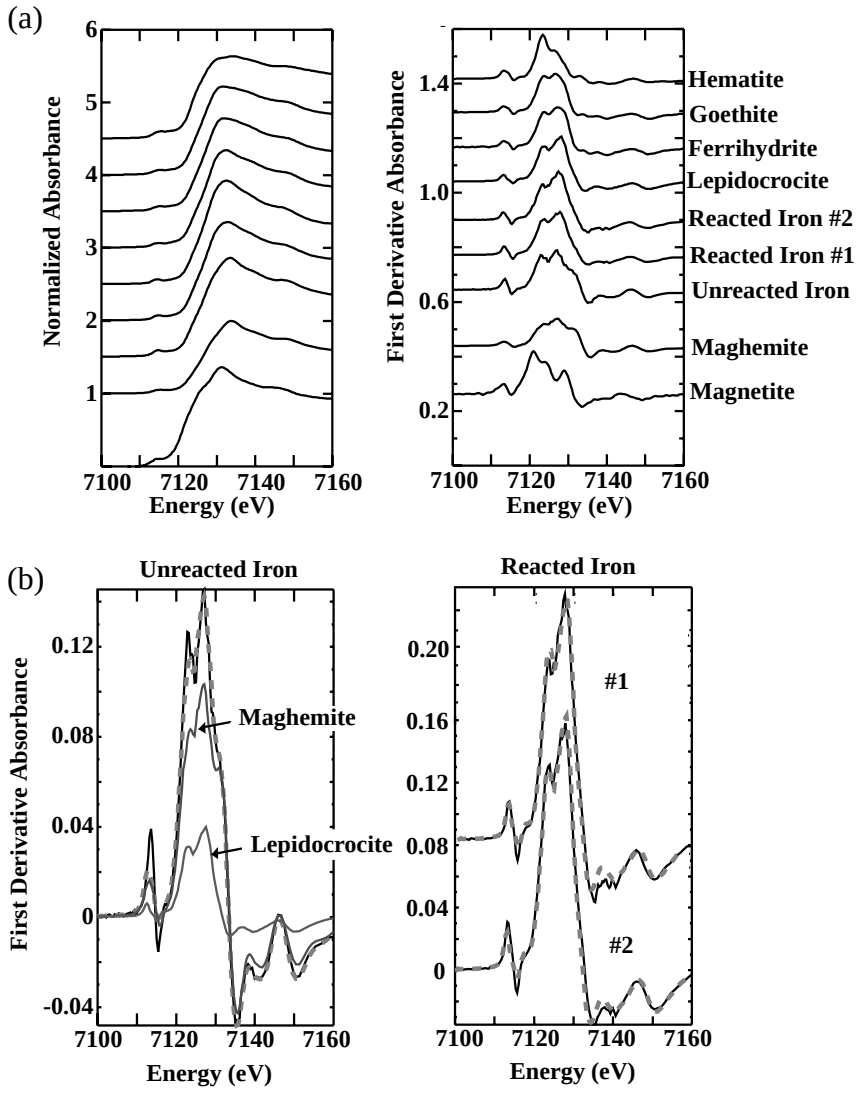

Figure 3. (a) Iron K-edge XANES spectra of reacted and unreacted column samples compared with reference compounds; (b) Fits of 1st–derivative spectra with maghemite and Fe(III) oxyhydroxide (lepidocrocite) reference spectra. Solid lines are data; dashed lines are least-squares fits.

Figure 4 shows the EXAFS spectra and best fits of unreacted and reacted column samples compared to the reference compounds identified in the XANES analysis. Numerical fit results are summarized in Table 2. The reacted sample has distinct differences in its EXAFS when compared to the unreacted sample spectrum. In the unreacted iron spectra, there is a small shoulder on the first peak at k = 5.5 $Å^{-1}$ which matches maghemite and is not present in the reacted iron #1 spectra. Also, oscillations from k = 9-11.2 $Å^{-1}$ are weaker in unreacted iron. Although similar, the unreacted sample spectrum does not exactly match the reference maghemite spectrum, consistent with the XANES fit result that indicated a second, small component of Fe(III) oxyhydroxide.

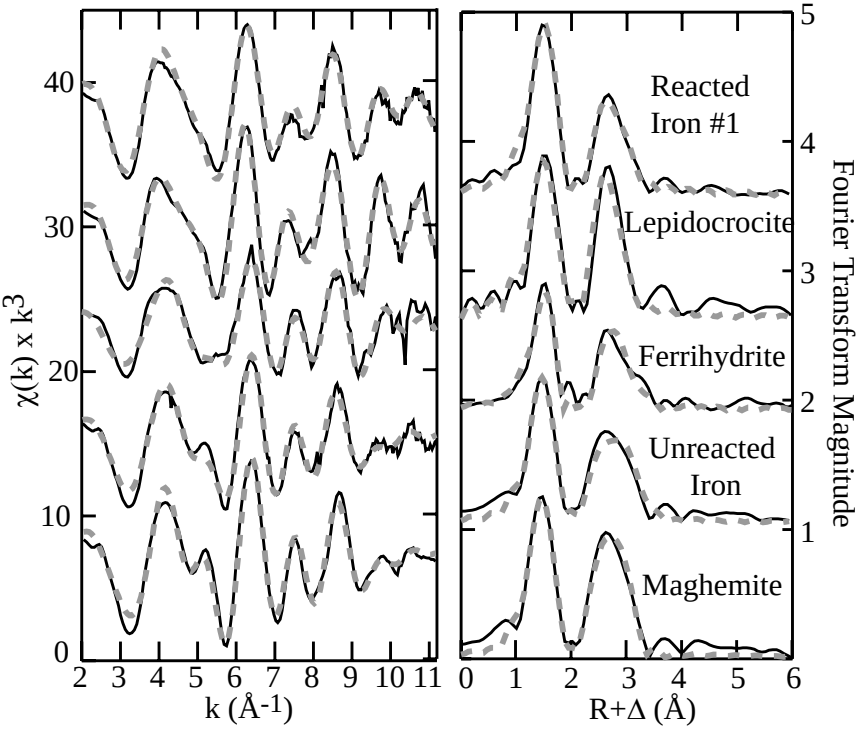

Figure 4. Iron K-edge EXAFS spectra. EXAFS spectra and corresponding Fourier transforms for reacted and unreacted column samples compared with reference compounds. Solid lines are data; dashed lines are least-squares fits.

The EXAFS spectrum of the reacted sample was fit assuming interatomic distances that were consistent with an Fe(III) oxyhydroxide local structure. However, fits assuming only the local structure of either lepidocrocite or ferrihydrite did not adequately fit the spectrum (note that the EXAFS spectrum

of goethite is nearly identical to that of ferrihydrite, see *14*). Bulk analysis of the reacted samples for As (Table 1) suggest that a relatively high concentration of As was associated with the reacted iron. Thus, the fit model was modified to include As in the local atomic structure. Least-squares refinement of the EXAFS indicated a small fraction of backscattering from arsenic (N ~ 0.8) at a mean distance of 3.34 (±0.02) Å (Table 2). The Fe-Fe interatomic distances determined in the fit are more similar to the local structure of lepidocrocite than ferrihydrite, with two distances resolvable at 2.97 Å and 3.08 Å. The Fe-As interatomic distance from the EXAFS fit is slightly longer than the distance reported in laboratory studies of arsenate sorbed to lepidocrocite (R = 3.34 ±0.02 Å vs. R = 3.29 Å from (*11*)) but within error of the Fe-As distance in the mineral scorodite ($FeAsO_4 \cdot 2H_2O$) as determined by EXAFS (R = 3.35-3.36 Å from (*11*) and (*17*)). This interatomic distance indicates a local geometry in which an arsenate tetrahedron forms a bridging bidentate complex to two iron octahedra (*11,18,19*). Based on the amount of As in the reacted sample and the local geometry determined by EXAFS, we postulate that new reactive sites are produced as the material reacts with the water, maghemite is oxidized, and an Fe(III) solid precipitates, incorporating sorbed As into the local structure. Incorporation of As into the newly formed Fe(III) oxyhydroxide would cause local disorder of the ideal structure, and therefore explain why the observed spectrum of the reacted sample does not match the local atomic structure of either lepidocrocite or ferrihydrite.

SEM imaging of reacted media showed precipitates forming on both ZVI particles and quartz grains (Figure 5). Silicon (from quartz sand) and Fe were detected by EDS spot analyses but As was not, probably because EDS is not particularly surface sensitive, and As may not be uniformly distributed in the reacted iron particles.

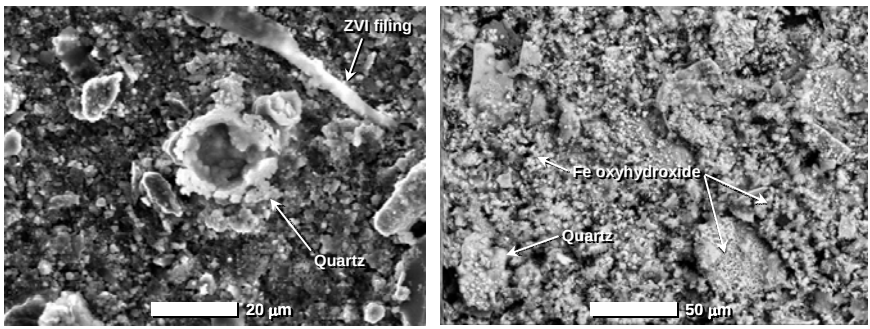

Figure 5. SEM images of ZVI/quartz media. Left: unreacted media showing ZVI filings and quartz particles. Right: reacted media showing extensive formation of iron-oxyhydroxides both as discrete particles and as surface precipitates on quartz.

Table 2. EXAFS fit results for unreacted and reacted iron compared to reference compound fits.

Sample	*A-B*	N_B	*R (Å)*	σ^2 *(Å^2)*	ΔE_0 *(eV)*	χ^2	
Unreacted Iron	Fe-O	2.2*	1.91*	0.0045*	0.3*	0.23	
	Fe-O	2.9*	2.02*	0.0088*			
	Fe-Fe	3.1*	2.99*	0.0099*			
	Fe-Fe	4.2*	3.47*	0.0110*			
	Fe-Fe	1.0*	3.71*	0.0027*			
Reacted Iron #1	Fe-O	6	1.98*	0.0094*	-0.3*	0.23	
	Fe-Fe	1.6*	2.97*	0.0094*			
	Fe-Fe	2.6*	3.08*	0.0070*			
	Fe-As	0.8*	3.34*	0.0060*			
Reference Compounds	*A-B*	N_B	*R (Å)*	σ^2 *(Å^2)*	ΔE_0 *(eV)*	χ^2	*Crystallographic R (Å)*
Lepidocrocite[a]	Fe-O	6	1.99*	0.0069*	1.0*	0.55	2.01
	Fe-Fe	4	3.03*	0.0094*			2.94
	Fe-Fe	2	3.07*	0.0030*			3.07
	Fe-Fe	2	3.98*	0.0080*			3.88
Ferrihydrite[b]	Fe-O	3	1.93*	0.0023*	-1.3*	0.11	
	Fe-O	3	2.05*	0.0058*			
	Fe-Fe	2	3.02*	0.0030*			
	Fe-Fe	2	3.24*	0.0015*			
	Fe-Fe	4	3.41*	0.0088*			
Maghemite[c]	Fe-O	1.3	1.92*	0.0046*	-0.35*	0.31	1.92, 1.98
	Fe-O	4	2.08*	0.0088*			2.08
	Fe-Fe	4	2.98*	0.0096*			2.96
	Fe-Fe	6	3.46*	0.0110*			3.42, 3.47
	Fe-Fe	1.3	3.69*	0.0030*			3.53

Notes: A-B is the absorber-backscatterer atom pair; N_B = number of backscatterers at interatomic distance R; σ^2 is the Debye-Waller factor; ΔE_0 is the difference in photoelectron threshold energy between reference functions and data; χ^2 is a reduced least-squares goodness-of-fit parameter. The amplitude reduction factor (S_o^2) was fixed at 0.70 for all samples except for ferrihydrite (varied value = 0.26, see (*14*)) and lepidocrocite (varied value = 0.74 with N fixed). Crystalline reference compounds lepidocrocite and maghemite are compared to interatomic distances determined independently by X-ray diffraction.

*Parameter varied in least squares fit; for fits with large number of shells, parameters not all varied simultaneously.

[a]Crystallographic distances calculated from the structure determination of (*20*).

[b]Reference compound fit from (*14*).

[c]The two crystallographic R values represent tetrahedral Fe^{IV} and octahedral Fe^{VI} in maghemite (21).

In-Ground Reactor

The prototype reactor treated nearly 4,000,000 L or approximately 4,400 pore volumes (PV) of contaminated groundwater over the course of the one-year test period at flow rates typically between 5 and 12 L/min. The reactor was not operated between days 109 (~1,180 PV) and 197 due to lack of groundwater flow to the reactor caused by declining groundwater levels.

A typical profile of changes in water chemistry inside the reactor is shown in Figure 6. Dissolved oxygen and arsenic are rapidly depleted within the first 30 cm of the ZVI bed, and dissolved iron increases. A significant increase in pH is also noted but was found to be inversely related to flow rate. Dissolved iron concentrations are highest within the ZVI bed and decrease again within the downstream gravel chamber due to continuing oxidation and precipitation.

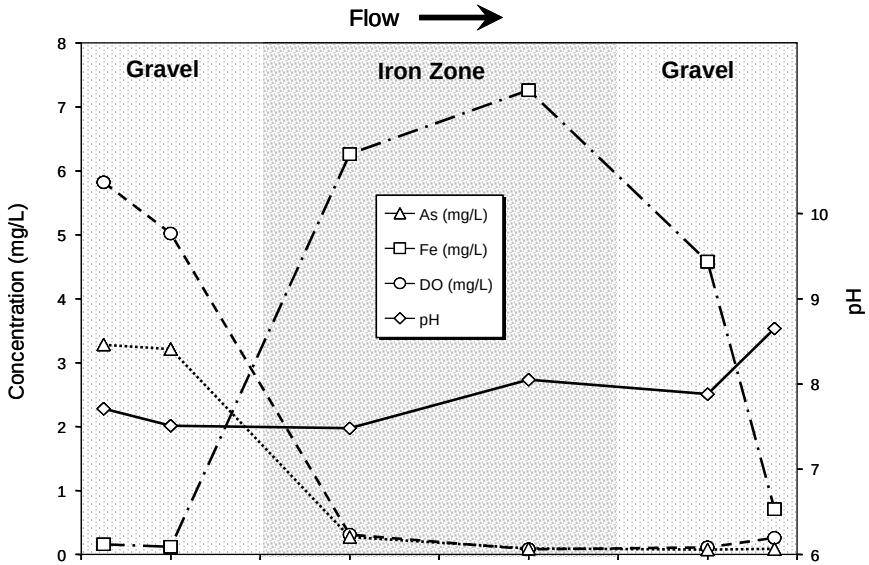

Figure 6. Cross-section of reactor showing typical profiles for dissolved arsenic, iron, and oxygen, and pH along the flowpath.

Influent dissolved As concentrations ranged from 2.26 to 3.46 mg/L with an average of 2.86 mg/L. Effluent dissolved As concentrations ranged from below analytical detection limits (2 μg/L) and increased over time to greater than 1 mg/L (Figure 7). Dissolved As concentrations in monitoring points within the iron bed also increased over time but remained lower than the effluent.

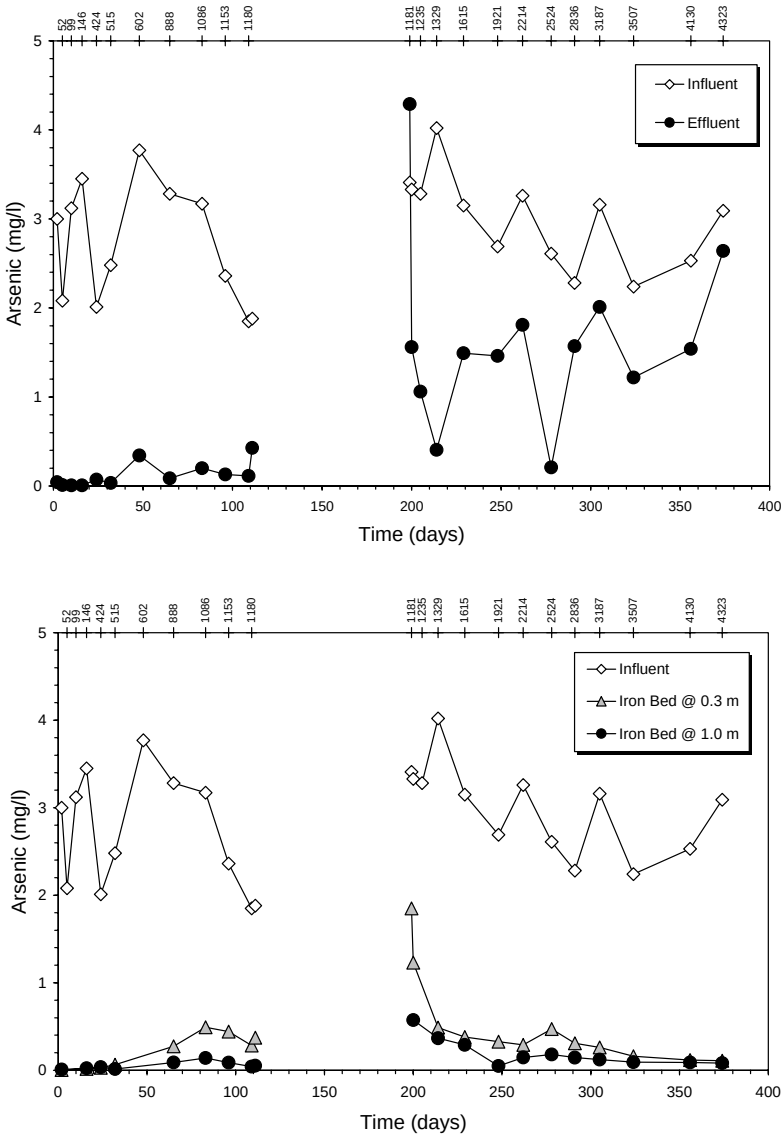

Figure 7. Time series of dissolved arsenic concentrations in influent, effluent (top), and interior monitoring points (bottom) of prototype reactor. Numbers across tops of graphs indicate number of pore volumes.

For a short time after the no-flow period ended (at day 198), elevated dissolved As concentrations and pH (10-12) were observed, both in the effluent and within the iron bed. This is explained by the prolonged contact time of the ZVI with stagnant water trapped in the reactor during the no-flow period (~88 days). Iron corrosion reactions progressed, creating a very high pH condition within the reactor. Arsenic adsorption on iron oxides and oxyhydroxides has a strong pH dependence (*22*), with the greatest adsorption occurring at near neutral to slightly basic pH and decreasing with increasing pH above 8-9. Therefore, high pH within the stagnant reactor caused temporary desorption of previously adsorbed As. After the stagnant water was flushed by new groundwater, arsenic concentrations within the iron bed again decreased to levels observed prior the no-flow period (Figure 7).

Following ~1,300 PV, effluent concentrations became more erratic, and began to approach influent concentrations. This was accompanied by a gradual increase in the hydraulic head gradient across the upstream front of the iron bed over time. It was hypothesized that preferential flow pathways had formed within the reactor. A tracer test subsequently confirmed that part of the flow was bypassing the iron bed. Examination of monitoring data indicated significant flow bypassing had started between approximately 1,600 and 2,200 PV.

Measured Eh-pH conditions within the reactor fall into the stability fields of Fe(III) oxyhydroxide and As(V) (Figure 8), which have also been confirmed by XANES and EXAFS spectroscopy (arsenic spectroscopic data not presented here).

Conclusions

The combination of field test results as a function of flow rate and spectroscopic characterization indicate molecular-level reactions that influence the performance of iron reactive barriers for arsenic removal. Our observations are consistent with a mechanism of arsenic uptake that is not limited by the surface sorption capacity of the solid, but instead reflects a balance between the rate of oxidation of maghemite to Fe(III) oxyhydroxide, and the rate of As incorporation into the newly formed oxyhydroxide. Flow rate is important in determining the extent of As uptake because it determines the loading rate of arsenic, the rate of supply of oxidants (dissolved oxygen), and the residence time for reaction with iron media. Although the initial arsenic adsorption step is relatively fast, sufficient residence time is needed to achieve a particular effluent concentration. Long residence times, however, can also lead to higher pH and less efficient As adsorption onto Fe(III) oxyhydroxide. This is a particularly important consideration for passive (*in situ*) applications where natural variations in flow rate may be significant.

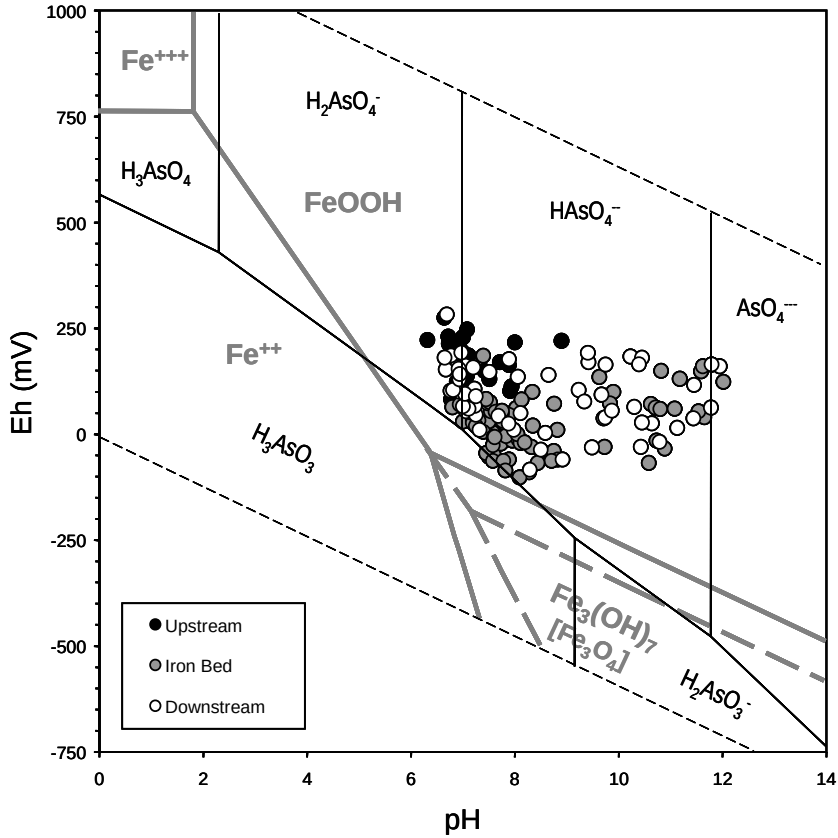

Figure 8. Measured Eh-pH relations within the iron bed and in the upstream and downstream gravel chambers plotted on an Eh-pH diagram showing stability regions of dissolved arsenic species (black lines) and iron oxide/hydroxides (thick gray lines). Green rust ($Fe_3(OH)_7$) field shown by solid gray lines and magnetite (Fe_3O_4) field shown by dashed lines. Thermodynamic data for arsenic species from (23), and for green rust and other iron species from (24).

References

1. *Handbook of Groundwater Remediation Using Permeable Reactive Barriers;* Naftz, D; Morrison, S.J.; Fuller, C.C.; Davis, J.A., Eds.; Academic Press: San Diego, CA, 2002, 539 p.
2. Lackovic, J.A.; Nikolaidis, N.P.; Dobbs, G.M. *Environ. Eng. Sci*. **2000**, *17*, 29-39.
3. Su, C.; Puls, R.W. *Environ. Sci. Technol.* **2001**, *35*, 1487-1492.
4. Farrell, J.; Wang, J.; O'Day, P.; Conklin, M. *Environ. Sci. Technol.* **2001**, *35*, 2026-2032.
5. Melitas, N.; Wang, J.; Conklin, M; O'Day, P.; Farrell, J. *Environ. Sci. Technol.* **2001**, *35*, 2074-2081.
6. Vlassopoulos, D.; Pochatila, J.; Lundquist, A.; Andrews, C.B.; Rafferty, M.T.; Chiang, K.; Sorel D.; Nikolaidis, N.P. In *Remediation of Chlorinated and Recalcitrant Compounds—2002*; Gavaskar, A.R.; Chen, A.S.C., Eds.; Battelle Press: Columbus, OH, 2002; Paper 2H-05.
7. Nikolaidis, N.P.; Dobbs, G.M.; Lackovic, J.A. *Water Research* **2003**, *37*, 1417-1425.
8. Randall, S.R.; Sherman, D.M.; Ragnarsdottir, K.V. *Geochim. Cosmochim. Acta* **2001**, *65*, 1015-1023.
9. Su, C.; Wilkin, R.T. **2005**, In *Advances in Arsenic Research*; O'Day, P.; Vlassopoulos, D.; Meng, X.; Benning, L., Eds.; ACS Symposium Series; American Chemical Society: Washington, DC, 2002; this volume.
10. Fuller, C.C.; Davis, J.A.; Waychunas, G.A. *Geochim. Cosmochim. Acta* **1993**, *57*, 2271-2282.
11. Waychunas, G.A.; Rea, B.A.; Fuller, C.C.; Davis, J.A. *Geochim. Cosmochim. Acta* **1993**, *57*, 2251-2269.
12. George, G.N.; Pickering, I.J. *EXAFSPAK: A suite of computer programs for analysis of X-ray absorption spectra*; Stanford Synchrotron Radiation Laboratory: 2000.
13. Rehr, J.J.; Albers, R.C.; Zabinsky, S.I. *Phys. Rev. Lett.* **1992**, *69***,** 3397–3400.
14. O'Day, P.A., Rivera, N., Root, R. & Carroll, S.A. *Am. Mineral.* **2004**, *89*, 572–585.
15. Brown, G.E.; Calas, G.; Waychunas, G.A.; Petiau, J. In *Spectroscopic Methods in Mineralogy and Geology*; Hawthorne, F. C., Ed.; Mineralogical Society of America: Washington, DC, 1988; Vol. 18, p 431-512.
16. O'Day, P.A., Rehr, J.J., Zabinsky, S.I.; Brown, G.E., Jr. *J. Am. Chem. Soc.* **1994**, *116*, 2938–2949.
17. Foster, A.L.; Brown, G.E., Jr.; Tingle, T.N.; Parks, G.A. *Am. Mineral.* **1998**, *83*, 553-568.

18. Savage, K.E.; Tingle, T.N.; O'Day, P.A.; Waychunas, G.A.; Bird, D.K. *App. Geochem.* **2000**, *15*, 1219-1244.
19. Foster, A.L; In *Arsenic in Goundwater;* Welch, A.H.; Stollenwerk, K.G., Eds.; Kluwer: Boston, MA, 2003; pp. 27–65.
20. Christensen, A.N.; Lehmann, M.S.; Convert, P. *Acta Chem. Scan. Ser. A* **1982**, *36*, 303-308.
21. Greaves, C. *J. Solid State Chem.* **1983**, *30*, 257-263.
22. Dixit, S.; Hering, J. *Environ. Sci. Technol.* **2003**, *37*, 4182-4189.
23. Nordstrom, D.K.; Archer, D.G. In *Arsenic in Goundwater;* Welch, A.H.; Stollenwerk, K.G., Eds.; Kluwer: Boston, MA, 2003; pp. 1–25.
24. Bourrié, G.; Trolard, F.; Genin, J.M.R.; Jaffrezic, A.; Maitre, V.; Abdelmoula, M. *Geochim. Cosmochim. Acta* **1999**, *63*, 3417–3427.